

Radiation Environment of the Chandra X-ray Observatory

S. L. O'Dell^a, M. W. Bautz^b, W. C. Blackwell^c, Y. M. Butt^d, R. A. Cameron^d,
R. F. Elsner^a, M. S. Gussenhoven^e, J. J. Kolodziejczak^a, J. I. Minow^c, R. M. Suggs^f,
D. A. Swartz^g, A. F. Tennant^a, S. N. Virani^d, and K. Warren^h

^a NASA Marshall Space Flight Center, MSFC/SD50
Huntsville, AL 35812 USA

^b Massachusetts Institute of Technology, Center for Space Research
Cambridge, MA 02139 USA

^c Sverdrup Technology Incorporated, MSFC/ED44
Huntsville, AL 35812 USA

^d Harvard-Smithsonian Center for Astrophysics, 60 Garden Street
Cambridge, MA 02138 USA

^e Air Force Research Laboratory, Space Hazards Branch, AFRL/VSBS
Hanscom AFB, MA 01731-3010 USA

^f NASA Marshall Space Flight Center, MSFC/ED44
Huntsville, AL 35812 USA

^g Universities Space Research Association, MSFC/SD50
Huntsville, AL 35812 USA

^h Raytheon Technical Services Company, MSFC/ED44
Huntsville, AL 35812 USA

ABSTRACT

The *Chandra* X-ray Observatory, the x-ray component of NASA's Great Observatories, provides unprecedented subarcsecond imaging, imaging spectrometry, and high-resolution dispersive spectroscopy of cosmic x-ray sources. During the initial phase of operation, some of the focal-plane charge-coupled devices (CCDs) — namely, the front-illuminated devices — experienced an unanticipated increase in charge-transfer inefficiency (CTI). Investigation of this anomaly determined the root cause to be radiation damage by weakly penetrating protons, entering the telescope's aperture and scattered off the mirrors into the focal plane. Subsequent changes in operating procedures have slowed the rate of increase of the CTI of the front-illuminated CCDs to acceptable levels. There has been no measurable degradation of the back-illuminated CCDs.

Keywords: radiation, protons, CCDs, space environment, space missions.

1. INTRODUCTION

The *Chandra* X-ray Observatory^{1,2} — formerly, the Advanced X-ray Astrophysics Facility^{3,4} (AXAF) — is the x-ray counterpart to the *Hubble* Space Telescope. Built by prime contractor TRW, managed by NASA's Marshall Space Flight Center (MSFC), and operated by the Smithsonian Astrophysical Observatory (SAO), *Chandra* (Figure 1) represents a unique facility for high-resolution imaging and spectroscopy of cosmic x-ray sources. Key features of the Observatory are x-ray optics of unprecedented, subarcsecond resolution, two sets of interchangeable objective transmissions gratings (OTGs), and two interchangeable focal-plane high-resolution imaging instruments. Each of the two focal-plane instruments provides two sets of detectors — one optimized for direct imaging, the other for read-out of dispersed spectra. The High-Resolution Camera^{5,6} (HRC, developed by the Smithsonian Astrophysical Observatory) employs microchannel plates; the Advanced CCD Imaging Spectrometer^{7,8} (ACIS, developed by Pennsylvania State University and the Massachusetts Institute of Technology) uses charge-coupled devices (CCDs, Figure 1).

Contact information:

S.L.O.: E-mail = Steve.O'Dell@msfc.nasa.gov; Phone = 1-256-544-7708; Fax = 1-256-544-7754.

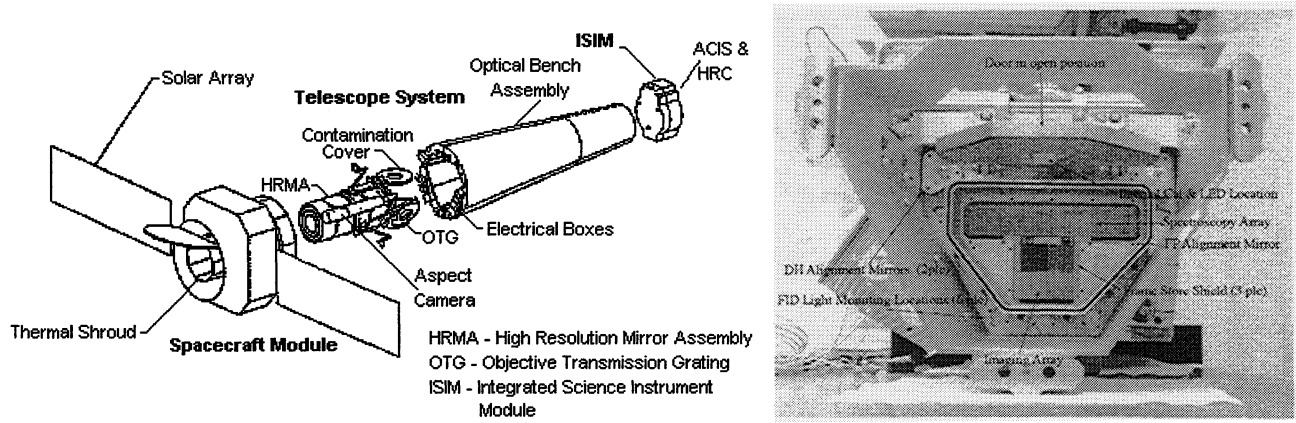


Figure 1. *Chandra* X-ray Observatory (left) and ACIS (right). Principal observatory components are the High-Resolution Mirror Assembly (HRMA), the two Objective Transmission Gratings (OTGs), and the Integrated Science Instrument Module (ISIM). On a translation table within the ISIM, reside the two focal-plane instruments — the Advanced CCD Imaging Spectrometer (ACIS) and the High-Resolution Camera (HRC). The ACIS focal plane (shown without optical blocking filters) contains 4 CCDs in the square Imaging (I) array and 6 CCDs in the rectangular Spectroscopy (S) array. Two of the S CCDs are back-illuminated devices; all other CCDs are front-illuminated.

On 1999 July 23, the National Aeronautics and Space Administration (NASA) launched the *Chandra* X-ray Observatory, on the space shuttle *Columbia*, as the STS-93 mission. After deployment from the orbiter, only about 8 hours after launch, an Inertial Upper Stage (IUS, by Boeing) and then an Integral Propulsion System (IPS, by TRW) placed *Chandra* into its operational orbit, with the final IPS burn on 1999 August 9. To optimize observing time, the operational orbit (Figure 2) is highly elliptical (10,000-km perigee by 140,000-km apogee), with a 63.5-hour period. In such an orbit, about 80% of the time — namely, the portion of the orbit outside the radiation belts — is available for observing cosmic x-ray sources. On 1999 August 12, the sun-shade door and forward contamination cover opened (Figure 1), for the *Chandra* focal planes's first exposure to cosmic x-rays and the space environment. The *Chandra* x-ray images (see, e.g., Reference 2) are spectacular!

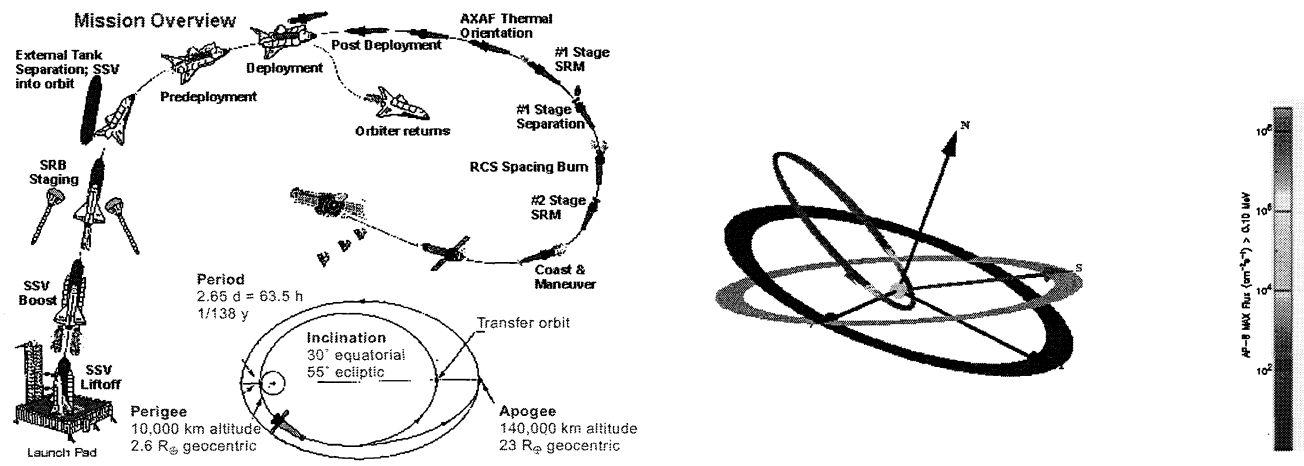


Figure 2. *Chandra* X-ray Observatory orbit. After deployment from the shuttle orbiter *Columbia*, an Inertial Upper Stage (IUS), then an Integral Propulsion System (IPS) placed *Chandra* in its highly elliptical — 10,000-km-altitude perigee and 140,000-km-altitude apogee — operational orbit (left). In this orbit, *Chandra* traverses the outer radiation belt and thus experiences a high-flux proton environment during perigee passes (right, generated using the SPENVIS⁹ tool).

Within about one month of the door opening, analysis of the ACIS spectra showed that the energy resolution of the front-illuminated CCDs was rapidly degrading. Fortunately, the *Chandra* team identified the cause of this degradation — damage by weakly penetrating radiation (protons or other ions) — and implemented procedures which have slowed the rate of loss of energy resolution to acceptable levels. Here, we give an overview of the status, beginning with a description of the charge-transfer inefficiency (CTI) anomaly^{10,11} (§2). Next we discuss pre-flight and post-anomaly analyses of the radiation environment¹² (§3) and of shielding and ion transport¹³ (§4). We conclude with a brief report on the mitigation strategies (§5) which have succeeded in reducing the rate of increase of the CTI.

2. CTI ANOMALY

When in the next-in-line (NIL) position, radioactive sources mounted on the Science Instrument Module (SIM), irradiate the ACIS focal plane. The iron-55 (Fe^{55}) electron-capture source produces 3 strong lines — direct emission from the manganese ($Mn-K\alpha$, 5.90 keV) daughter, plus fluorescence of titanium ($Ti-K\alpha$, 4.51 keV) and of aluminum ($Al-K\alpha$, 1.49 keV) targets. Analysis of the event lists allows calibration of energy scale (gain), energy resolution, and quantum efficiency of the CCDs, as a function of position. The CCD-row dependence of gain results from charge loss during parallel read-out into the frame-store area; that of energy resolution, from fluctuations in charge loss.

First, we briefly review the history of the CTI anomaly (§2.1) and the anomaly investigation (§2.2). Then, we discuss the root cause of the CTI increase (§2.3) and the current status of the front-illuminated CCDs (§2.4).

2.1. History

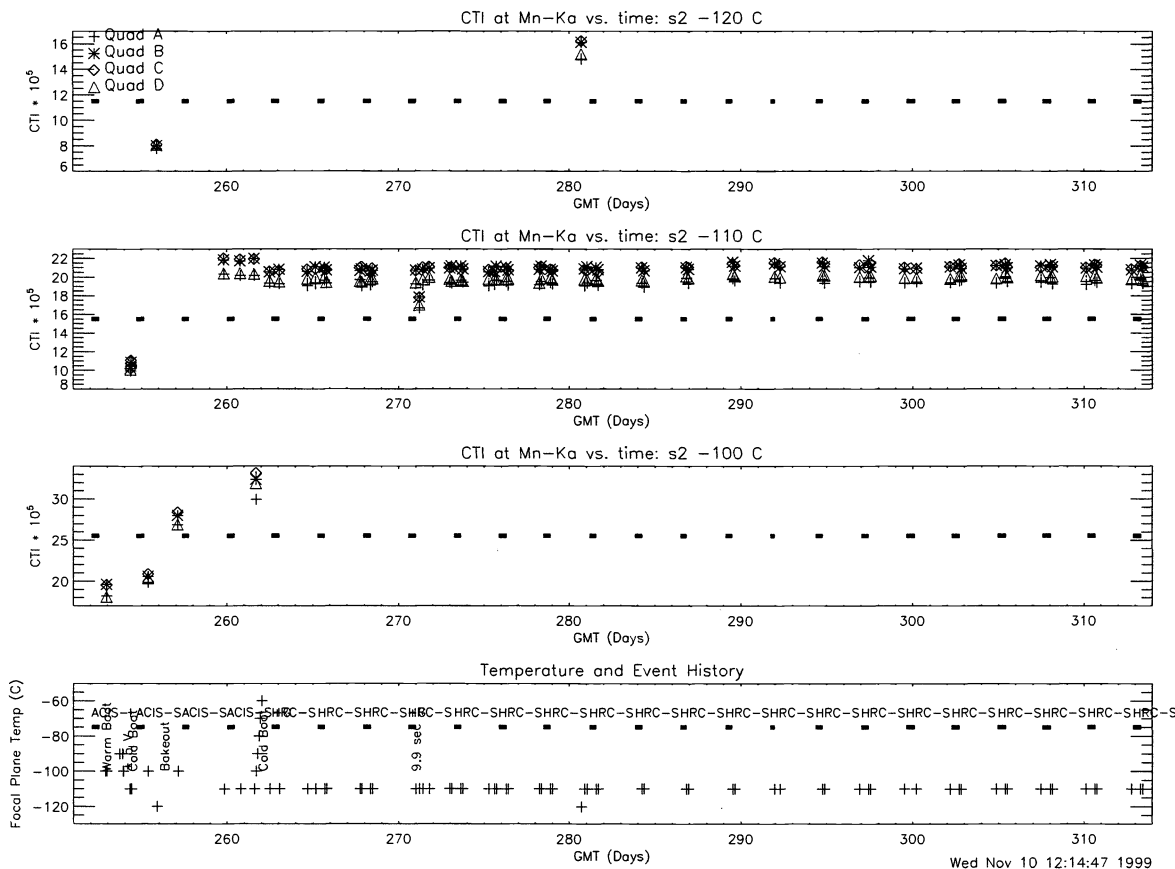


Figure 3. History of Charge Transfer Inefficiency (CTI) of an ACIS front-illuminated CCD — S2. During the first eight unprotected perigee passes, the CTI of the ACIS eight front-illuminated CCDs increased from about 10^{-6} to 2×10^{-4} (at $-110^{\circ}C$, for 5.9-keV photons). Hiding the ACIS during perigee passes has significantly slowed this CTI increase, to about 5% of its current value per year. (CTI plots are by Catherine Grant, of the ACIS team at MIT.)

On 1999 September 9, analysis of ACIS event histograms revealed a substantial increase in the full-width-at-half-maximum (FWHM) energy resolution of the front-illuminated CCDs. Examination of the calibration data showed that the charge-transfer inefficiency (CTI) of the front-illuminated devices (Figure 3) had increased by about two orders of magnitude since ground calibration. On the other hand, there was no indication of an increase in the CTI of the back-illuminated devices (Figure 4). Thus, the CTI of the front-illuminated CCDs had increased from about 10^{-6} to about 10^{-4} , while the CTI of the back-illuminated CCDs had remained at about 10^{-5} .

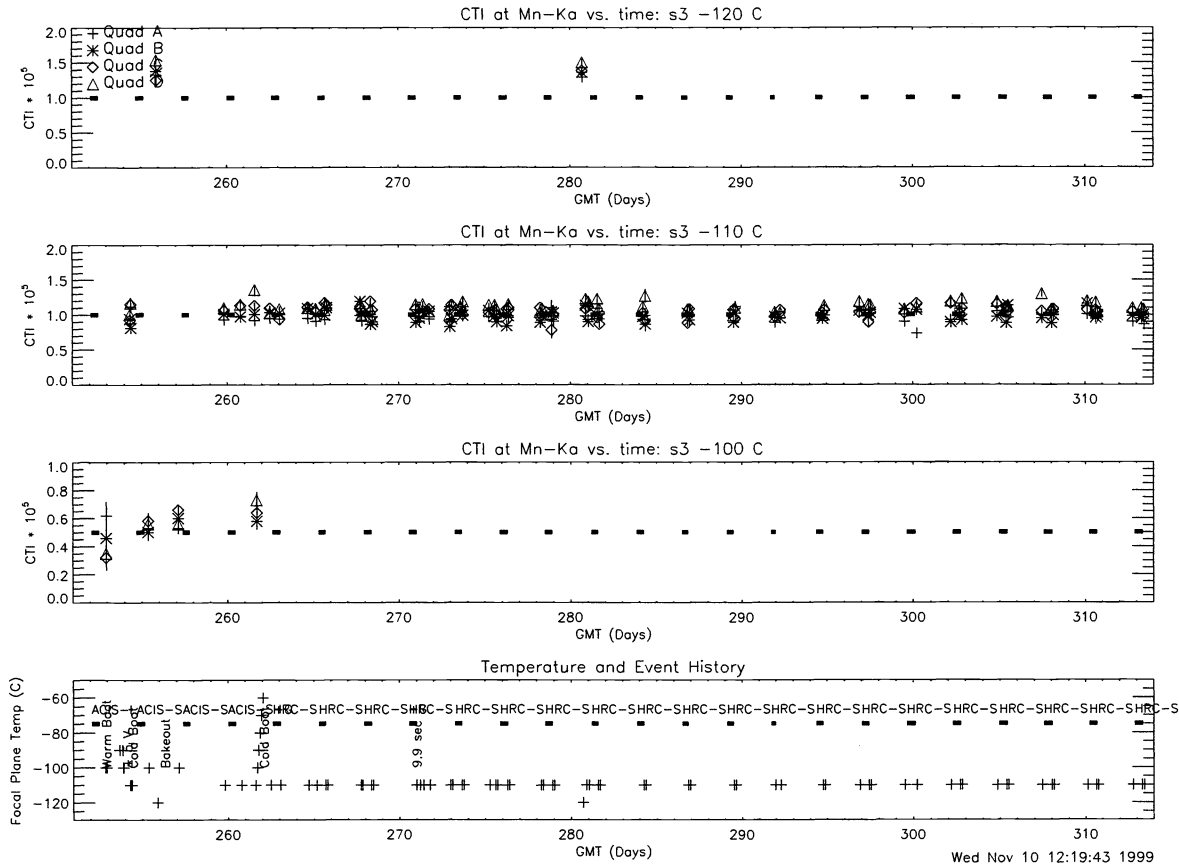


Figure 4. History of Charge Transfer Inefficiency (CTI) of an ACIS back-illuminated CCD — S3. The CTI of the ACIS two back-illuminated CCDs has remained essentially unchanged, at about 10^{-5} (at -110°C , for 5.9-keV photons), since prior to launch. (CTI plots are by Catherine Grant, of the ACIS team at MIT.)

During the next couple weeks, it became clear that large CTI increases occurred only when ACIS was in the observing position during radiation-belt passages. When, during radiation-belt passages, ACIS was in the next-in-line (NIL) position or the High-Energy Transmission Grating^{14,15} (HETG, developed by the Massachusetts Institute of Technology) was inserted, there was no measurable CTI increase. With this knowledge, the *Chandra* team changed operating procedures (§5) to move ACIS into the NIL position for all radiation-belt passages. Baseline operating procedures had left the current observing instrument (ACIS or HRC) in the focal position, with its door open, during belt passages, in order to minimize use of mechanisms. By moving the ACIS into the NIL position during all radiation passes (and severe solar-proton storms, §3), the *Chandra* team has succeeded in halting the rapid degradation of the front-illuminated CCDs, so that the devices remain scientifically useful.

2.2. Anomaly investigation

Upon discovery of the unanticipated CTI increase, the *Chandra* Project convened a CTI-anomaly investigation. Lincoln Laboratories, which designed and fabricated the CCDs, hosted the first meeting, about two weeks after

recognition of the CTI anomaly. This meeting brought together experts in charge-coupled devices, the radiation environment, and spacecraft anomalies. In response to the anomaly, the *Chandra* Project then established a CTI Task Team, which includes two principal investigating teams:

1. The CCD Team, led by the ACIS team at MIT, has characterized the CTI increase in the flight CCDs,¹⁰ conducted laboratory experiments on flight-like CCDs, and investigated CCD modes of operation which might recover some of the original resolving power.^{10,11}
2. The Radiation Team, led by *Chandra* Project Science at MSFC, re-analyzed assumptions about the radiation environment (§3) and the shielding calculations (§4), built a model of the radiation environment valid over the *Chandra* orbit¹² (§3), and developed simulations of ion transport through the optical system¹³ (§4).

2.3. Root cause

As the *Chandra* team was clarifying the nature of the CCD degradation and correlating the CTI increase with radiation-belt passages, it became clear that the probable cause was damage by weakly penetrating radiation. In particular, the prime suspect was and is moderately-low-energy (100–300 keV) protons (with possible contributions from helium and oxygen ions), irradiating the focal plane after single or double scattering off the telescope's x-ray mirrors. The evidence that the cause of the damage is weakly penetrating ions is quite convincing:

1. The back-illuminated CCDs, with the charge-transfer channel behind about 45 μm of silicon, have experienced no degradation of the energy resolution.¹⁰
2. Although the CTI of the front-illuminated CCDs increased dramatically, the dark current has not, indicating that the damage does not extend significantly beyond the charge-transfer channel of these devices.¹⁰
3. Serial-read-out (from the frame-store area) CTI is much less than parallel-read-out (into the frame-store area) CTI of the front-illuminated devices, showing that there has been no damage to the shielded frame-store area.¹⁰
4. With the HETG^{14,15} inserted, the CCDs experience little degradation, even when in the focal position during radiation-belt passages (§4).
5. When in the next-in-line (NIL) position during radiation-belt passages, the CCDs experience no degradation.
6. Analysis^{16,17} of ACIS spectra of Flight Contamination Monitor (FCM) sources^{18,19} mounted in the telescope's forward contamination cover, show no degradation of energy resolution prior to opening the sunshade door.
7. Irradiation (at Goddard Space Flight Center) of ACIS flight-like front-illuminated CCDs with 100–300-keV protons, reproduces the behavior of the ACIS flight devices.¹⁰

Previous experiences with radiation damage to CCDs^{20–22} had alerted the ACIS team to the risk of CCD degradation by protons with energies of tens of MeV. Hence, during the development of AXAF, the *Chandra* Project and ACIS team made a concerted effort to shield against penetrating radiation (§4). Further, in order to monitor potentially damaging penetrating radiation, the AXAF incorporated the Electron, Proton, Helium Instrument²³ (EPHIN), developed by the University of Kiel (Germany) as a science instrument for the Solar and Heliospheric Observatory (*SOHO*). Unfortunately, we did not anticipate the radiation damage that the *Chandra* ACIS encountered — namely, radiation damage in the charge-transfer channel by moderately-low-energy (100–300-keV) protons, which reach the focal plane after scattering off the Observatory's grazing-incidence optics.

2.4. Status

Since adopting procedures to protect the ACIS CCDs from radiation damage by moderately-low-energy protons (§5), the CTI increase of the front-illuminated CCDs has slowed to an acceptable level. We believe that the current 5% annual rate of CTI increase is sustainable over the 5–15-year life of the mission (§3), without significant reduction in observing efficiency. Thus, the front-illuminated CCDs should remain scientifically useful throughout the *Chandra* mission. Further, the CTIs of the back-illuminated devices should remain nearly identical to their original values.

Meanwhile, the ACIS team continues to characterize the behavior of the CCDs.^{10,11} The primary goal now is to identify the traps and their associated time scales, in order to seek CCD operating modes which would improve the spectral resolving power of the front-illuminated devices.

3. RADIATION ENVIRONMENT

During the initial stages of the ACIS CTI anomaly investigation, we reviewed and independently repeated pre-flight analyses of the *Chandra* radiation environment. The investigation verified that the pre-flight models for the radiation environment, specified by Science Applications International Corporation (SAIC) with review by TRW and NASA, were essentially correct (Figure 5). However, because radiation damage by weakly penetrating protons scattering off the grazing-incidence mirrors was unexpected, the pre-flight shielding studies (§4) focussed on the known problem of radiation damage by strongly penetrating protons. Hence, the pre-flight concern about the radiation environment centered on solar energetic protons. This concern drove the pre-flight radiation-shielding studies (§4) and the selection of EPHIN²³ as the radiation monitor for the *Chandra* X-ray Observatory.

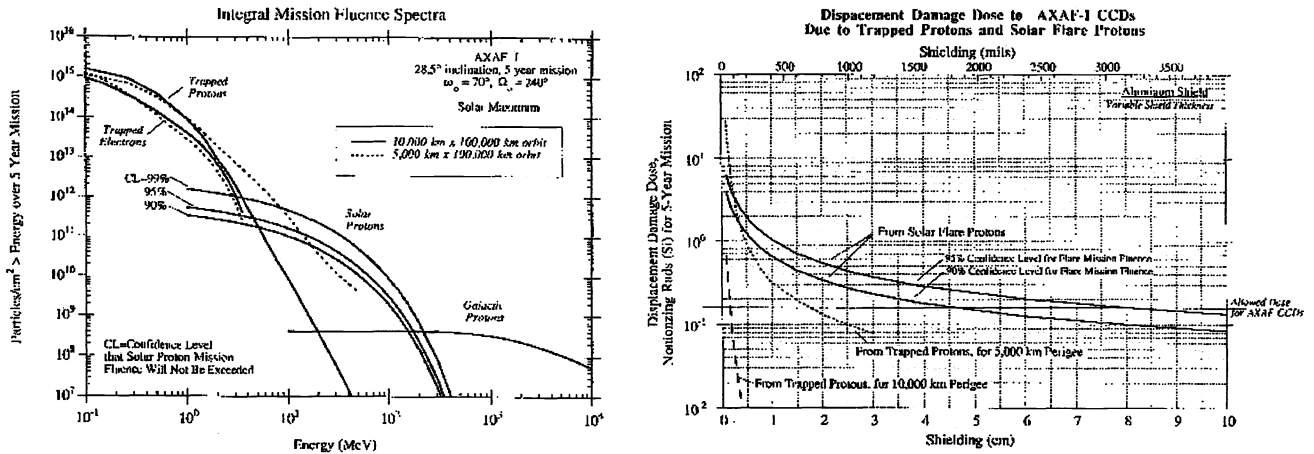


Figure 5. Some results of the pre-flight studies of the *Chandra* (AXAF) radiation environment. Primary contributors to the proton fluence (left) are trapped radiation at lower energies, solar energetic protons between several and a few hundred MeV, and Galactic cosmic rays at higher energies. Shielding against the strongly penetrating solar energetic protons drove the shielding design (right). (Plots are by Tony Armstrong, of SAIC.)

Upon realization that weakly penetrating protons (or other ions) were the probable cause (§2.3) of the unexpectedly rapid increase in the CTI of the ACIS front-illuminated CCDs (§2.1), it was immediately clear that these devices could not tolerate unprotected passages through the trapped-proton radiation belts. Hence, the *Chandra* team quickly modified operating procedures to, among other mitigation steps (§5), place the ACIS in the next-in-line (NIL) position for all radiation-belt passages. With the rapid CTI degradation halted, we began to define better the radiation environment for 100–300-keV protons. The motivations for doing so are these:

1. Independent of simulations of proton propagation through *Chandra*'s x-ray optical system (§4), one can scale CTI degradation to the external proton fluence. To normalize this scaling requires fairly accurate knowledge of the external proton fluence accumulated during unprotected passages of ACIS through the radiation belts.
2. The trapped-proton belts are the primary, but not the sole, contribution to the accumulated fluence of 100–300-keV protons. Thus, to hold further CTI degradation to tolerable levels requires understanding the radiation environment encountered throughout *Chandra*'s highly elliptical orbit.
3. To optimize performance (increase observing time, reduce CCD damage, and avoid autonomous radiation safing) requires an accurate radiation-environment model for planning events — configuring for radiation belts, hiding ACIS, inserting gratings, etc. Because the off-line system schedules events weeks in advance and the radiation environment is dynamic, mission planning must use probabilistic models for the radiation environment.
4. The National Oceanographic and Atmospheric Administration (NOAA) Space Environment Center (SEC) distributes real-time data on the solar, interplanetary, and geomagnetic environments. In responding to especially large increases in the proton flux, due to solar or geomagnetic activity, the model for the *Chandra* radiation environment must support near-real-time decisions whether to intervene and halt science observations.

By far, the largest contribution to the proton fluence in *Chandra's* orbit comes from the Earth's radiation belts. We computed the proton fluence for *Chandra's* orbit in the NASA AP8MAX environment, using the European Space Agency (ESA) SPENVIS⁹ (SPace ENVironment Information System) tool. As a cross-check, we also used the Air Force Research Laboratory (AFRL) CRRES-PRO tool,²⁴ with CRRES-EPAS (Combined Radiation and Release Effects Satellite - Electron Proton Angle Spectrometer) data sets. The EPAS Quiet model gives results very close to the AP8MAX one (Table 1); the Active model is nearly five (5) times higher than the results in Table 1. ACIS went unprotected through eight (8) radiation-belt passes, during relatively quiet periods. Consequently, the consensus estimate for the external proton fluence responsible for the observed CTI degradation, uses the AP8MAX (or nearly equal CRRES-EPAS Quiet) value. This value for the external proton fluence — 3.0×10^{12} p/(cm² sr MeV) at 0.14 MeV — constitutes the reference, with respect to which we normalize other contributions to the total proton fluence.

Although the AP8 model is adequate for assessing the proton fluence in the trapped radiation belts, its fidelity declines rapidly outside $6.6 R_{\oplus}$ geocentric (36-Mm altitude) — i.e., outside geosynchronous orbit.²⁵ Thus, we require other methods for estimating the proton flux over most of *Chandra's* highly elliptical orbit (Figure 2). The region of the magnetosphere immediately outside the classical radiation belts can quasi-trap particles. Using the CRRES Quiet and Active models, extrapolated using data from NASA's *Polar* mission, we determined the proton environments at $7.5\text{--}9 R_{\oplus}$ (41–51-Mm altitude) and at $9\text{--}11 R_{\oplus}$ (51–64-Mm altitude). Table 1 gives the mean value for the proton fluence accumulated as *Chandra* passes through each of these mid-magnetospheric regions. The ratio of the Active-model flux to the Quiet-model flux is about 2 between 7.5 and $9 R_{\oplus}$ and about 8 between 9 and $11 R_{\oplus}$. However, the duty cycle for activity is sufficiently small that, over the long term, the mean flux is much closer to the Quiet-model value than to the Active-model one.

Current operating procedures hide the ACIS from the entrance aperture before *Chandra* reaches this quasi-trapped region. These estimates demonstrate that this procedure must continue, in order to reduce the risk of further significant degradation of the ACIS front-illuminated CCDs. Given that the CCDs will no longer be exposed to weakly penetrating radiation below about $9\text{--}11 R_{\oplus}$, we must now examine the more distant radiation environment. The *Chandra* X-ray Observatory spends about 85%–80% of its time in this environment — the outer magnetosphere (including the magnetotail), the magnetosheath, and the solar wind. Because no comprehensive model for the proton flux in this more-distant and complicated environment existed, we have developed the *Chandra* Radiation Model.¹²

Table 1. Mean 0.14-keV proton fluence

Region	Radius [R_{\oplus}]	Time [%]	Orbital fluence [p/(cm ² sr MeV orb)]	Annual fluence [p/(cm ² sr MeV y)]	CTI rate [%/y]
Radiation belts	2.6–7.5	11	3.7×10^{11}	5.1×10^{13}	1700
Inner-mid magnetosphere	7.5–9	4	5.1×10^9	7.0×10^{11}	23
Outer-mid magnetosphere	9–11	5	5.4×10^8	7.5×10^{10}	2.5
Mean operational environment	> 9	86	1.3×10^9	1.7×10^{11}	5.9
	> 10	83	1.1×10^9	1.5×10^{11}	4.9
	> 11	80	9.1×10^8	1.3×10^{11}	4.2
	> 12	77	7.6×10^8	1.1×10^{11}	3.5
	> 13	74	6.5×10^8	8.9×10^{10}	3.0
	> 14	71	5.6×10^8	7.8×10^{10}	2.6
	> 15	67	4.8×10^8	6.6×10^{10}	2.2
Solar wind		100	4.6×10^8	6.4×10^{10}	2.1

The *Chandra* Radiation Model¹² is a data-driven model, based on approximately 5 years of data collected by the Energetic Particles and Ion Composition²⁶ (EPIC) instrument on the *Geotail* satellite,^{27,28} developed by the Japan Institute of Space and Astronautical Science (ISIS), with NASA. Since 1995, *Geotail* has operated in an elliptical orbit with an $8 R_{\oplus}$ perigee and $30 R_{\oplus}$ apogee. Thus, it samples a radiation environment similar to that of the *Chandra* X-ray Observatory — albeit at a lower orbital inclination. As reported in detail elsewhere,¹² the model — developed by Sverdrup Technology with the MSFC Space Environments group — provides a versatile description of the global radiation environment in the magnetosphere, magnetosheath, and solar wind. In addition to long-term-averaged mean, 50%, and 95% environments, the model can also represent the mean, 50%, and 95% environments for specified values of a geomagnetic index (such as the planetary K index, K_p).

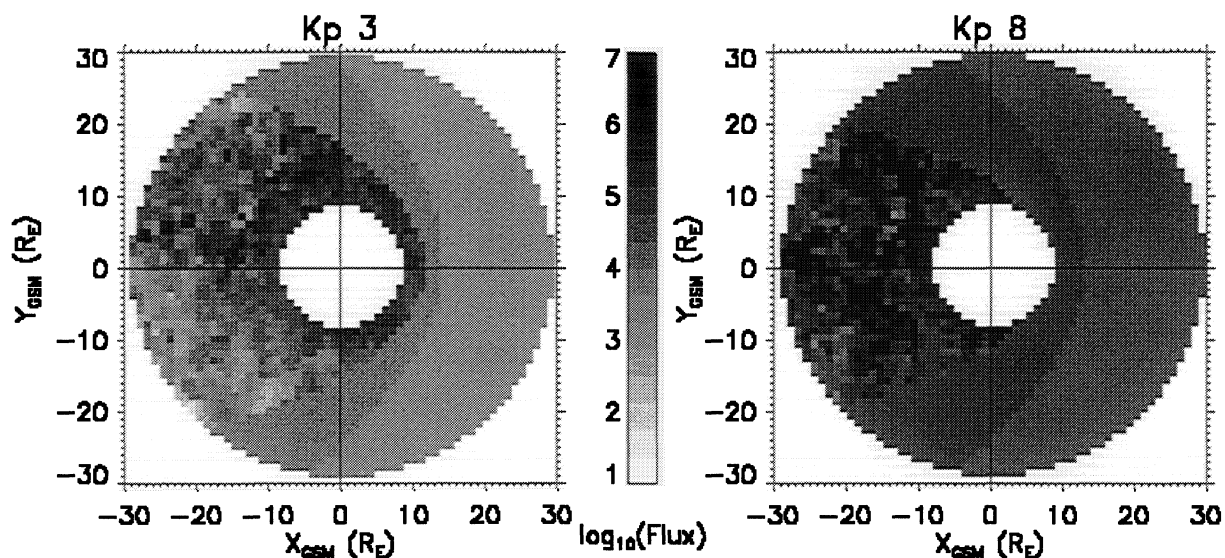


Figure 6. Omnidirectional spectral intensity of 100–200-keV protons outside the radiation belts. The maps, based on *Geotail* EPIC data, show the mean proton environment in the $Z_{\text{GSM}} = 0$ plane, for average geomagnetic activity ($K_p = 3$, left) and during a severe geomagnetic storm ($K_p = 8$, right). Clearly visible are the bow shock, magnetopause, and the concentration of protons in the tail-to-dusk sector of the outer magnetosphere. In Geocentric Solar Magnetic (GSM) coordinates, the Sun is in the $+X_{\text{GSM}}$ direction and the transverse projection of the Earth's north magnetic pole is in the $+Z_{\text{GSM}}$ direction. The proton spectral intensity, or “Flux”, is in $\text{p}/(\text{cm}^2 \text{ s sr MeV})$.

Figure 6 illustrates the distribution of 100–200-keV protons, in the 8–30- R_{\oplus} sampled by *Geotail*, for average and severe-geomagnetic-storm conditions. By propagating the *Chandra* orbit through a *Chandra* Radiation Model environment, we calculate the external proton flux and fluence. Due to the asymmetric proton distribution (Figure 6), there is a marked deterministic seasonal variation in *Chandra*'s exposure to the radiation environment, as the geotail sweeps around the Earth (in inertial coordinates). On shorter time scales, solar and geomagnetic activity drive changes in the environment. Table 1 gives the accumulated external fluence for the mean environment, averaged over a year, for various minimum operational radii.

Computer Sciences Corporation (CSC) is incorporating *Chandra* Radiation Model into the off-line software system, used by the *Chandra* X-ray Center (CXC) to schedule observations. With this tool, the planning system will optimize the schedule to decrease the accumulated proton fluence and increase observing time. The CXC nominally plans observations 3 weeks in advance, generates a one-week time line, uploads commands once a day, and downloads data 3 times a day during scheduled contacts through NASA's Deep Space Network (DSN). Because the CXC Operations Control Center is not usually in contact with the spacecraft, the mission planning must necessarily employ a probabilistic version of the model. However, the CXC does monitor the space environment, using near-real-time data provided by the National Oceanographic and Atmospheric Administration (NOAA) Space Environment Center (SEC). Thus, combined with these real-time data, the *Chandra* Radiation Model also provides a real-time tool for estimating proton flux and fluence accumulated in *Chandra*'s orbit. Using this information, the *Chandra* operations team can make near-real-time decisions regarding (§5) intervention to remove the ACIS from the focal position.

Especially valuable for *Chandra* operations has been near-real-time solar-wind monitoring,²⁹ using data from NASA's Advanced Composition Explorer³⁰ (*ACE*). In L1 orbit (0.01 Astronomical Units, or 235 R_{\oplus} , sunward of the earth, *ACE* provides a wealth of information on the solar-wind and interplanetary environment. The *ACE* Electron, Proton, and Alpha Monitor³¹ (EPAM) measures the intensity of moderate-energy (0.05–2-MeV) protons. In particular, the EPAM P3 channel, centered on about 0.14 MeV, measures the spectral intensity of protons believed to be most responsible for damaging the ACIS front-illuminated CCDs.

Besides giving direct information on the moderate-energy protons entrained in the solar wind headed toward the earth, other *ACE* instruments provide additional real-time information useful for *Chandra* operations. The *ACE*

Solar-Wind Electron Proton Alpha Monitor³² (SWEPAM) and the *ACE* Magnetic Fields Experiment³³ (MAG) measure the solar-wind plasma parameters. Using the *ACE*-derived solar-wind parameters, the SEC provides a prediction of geomagnetic activity through the Costello (neural-network) predictive K_p index.³⁴ The CXC can then use this geomagnetic index (or others) to evaluate the expected fluence within the *Chandra* Radiation Model.

Chandra operations also monitors SEC-provided measurements of the flux in Solar Energetic Particles (SEP), for information on penetrating radiation. The *ACE* Solar Isotope Spectrometer³⁵ (SIS) measures the flux of, among other species, high-energy (> 10 MeV) protons. Similarly, the SEC real-time proton-channel data from the NOAA Geostationary Operational Environmental Satellite (GOES) system describe the high-energy proton flux at 6.6 R_{\oplus} .

4. SHIELDING ANALYSES

During the initial stages of the ACIS CTI anomaly investigation, we reviewed and repeated pre-flight analyses of *Chandra* shielding. We developed higher fidelity geometric models of the spacecraft and carefully searched design drawings for sneak paths. The investigation verified that the pre-flight shielding studies, performed by Science Applications International Corporation (SAIC), using a geometric model developed by MSFC with inputs from TRW and the science-instruments teams, were essentially correct for strongly penetrating radiation (Figure 7). Indeed, the re-analysis, using the higher fidelity geometry, found that the shielding against penetrating radiation is somewhat better than found in the pre-flight analysis. However, because the shielding analyses considered only line-of-sight mass columns (Figure 7), they did not treat scattering of low-energy protons off the grazing-incidence mirrors. Nevertheless, they do show that shielding in the ACIS next-in-line (NIL) position is adequate to protect the front-illuminated CCDs from weakly penetrating radiation scattered by the telescope's x-ray mirrors. Treating the scattering requires a totally different approach¹³ from traditional quasi-one-dimensional shielding analyses.

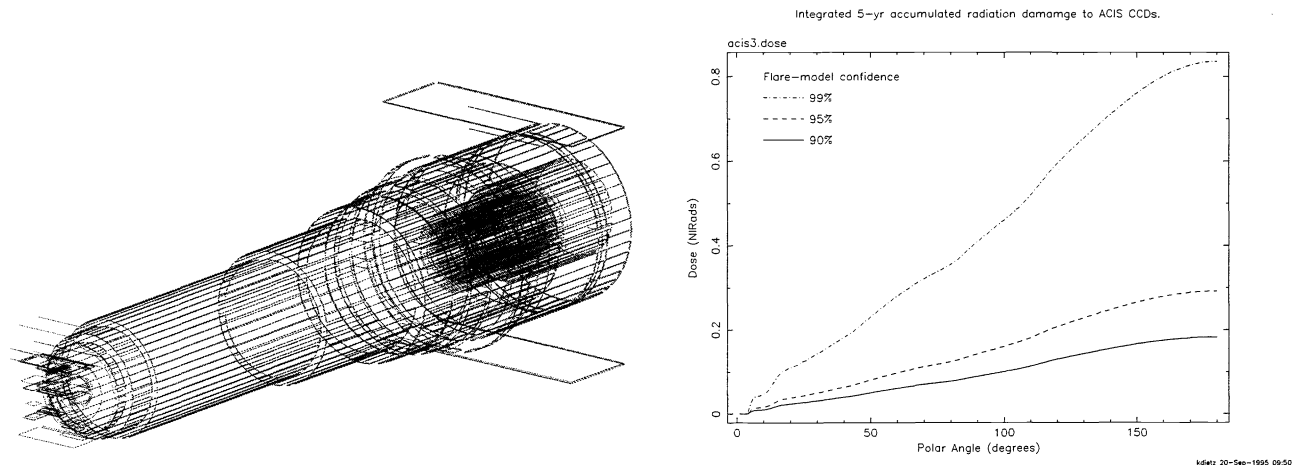


Figure 7. Spacecraft model and results of the pre-flight radiation analysis. With inputs from other members of the AXAF team, MSFC developed a geometric model of the spacecraft (left) for use in radiation-shielding analyses. Science Applications International Corporation (SAIC) and MSFC used the model to estimate the dose (right) of potentially damaging penetrating radiation on the ACIS CCDs.

Elsewhere¹³ we have reported simulations of the ion transport through the *Chandra* optical system. Using the simulation software Total Range of Ions in Matter³⁶ (TRIM) combined with the MSFC Project Science ray-trace code, we examined the relationship of focal-plane proton flux to the external omnidirectional flux. This study includes Rutherford scattering off the iridium-coated mirrors, transmission and dilution by the gratings (when inserted), transmission by the ACIS optical blocking filter, and transmission by the CCD structure above the critical charge-transfer channel. Given the deduced external proton fluence during unprotected radiation-belt passages (§3) and the damage sensitivity measured by proton irradiation of flight-like devices,^{10,11} the simulation somewhat underpredicts (by a factor of 3 or 4) the proton fluence at the focal position.¹³ In view of uncertainties in the simulation (especially in using TRIM at small grazing angles), in the radiation-environment estimates, and in the proton-irradiation measurements, we find this level of agreement acceptable. Note that operational decisions do not rely on the simulation results, instead they simply use scalings of the operational environments to the radiation belt.

5. MITIGATION STRATEGIES

The objectives of radiation protection are two-fold — to control the cumulative effects (primarily to the ACIS front-illuminated CCDs) of proton irradiation, and to avoid any immediate damage (primarily to the HRC microchannel-plate detectors and anti-coincidence phototubes) resulting from very high charged-particle rates. In order to ensure that the *Chandra* X-ray Observatory retains the scientific utility of the ACIS front-illuminated CCDs throughout the life of the mission and at the same time maintains high observing efficiency, we have budgeted a continued rate of CTI increase of 5%/y. The strategies for accomplishing these objectives are three-tiered.

5.1. Planning

Because *Chandra* observations are scheduled weeks in advance, the planning strategy uses probabilistic models for the radiation environment to determine when to protect the focal-plane instruments. The scheduling software will plan as much observing time as possible consistent with specified fluence and flux limits, plus an additional temporal pad to forestall autonomous safing (§5.3) near the radiation belts. In the near term, the planning system will use the AP8 model for flux thresholds and the *Chandra* Radiation Model for fluence thresholds. However, in the longer term, we shall expand the *Chandra* Radiation Model to include higher-energy *Geotail* EPIC proton channels for direct comparison with *Chandra*'s radiation monitor (EPHIN) channels. After accomplishing this, we expect the planning system will use the *Chandra* Radiation Model for flux, as well as fluence, thresholds.

5.2. Intervention

The intervention strategy uses near-real-time estimates of proton fluence and flux to assess whether to cease science operations at the next DSN contact or earlier. The *Chandra* operations team automatically monitors real-time data from the NOAA SEC (§3). Based upon the *Chandra* Radiation Model, upon *ACE* EPAM solar-wind proton levels and the *ACE*-driven Costello K_p predictor of geomagnetic activity, and upon the current spacecraft configuration, the CXC generates a near-real-time estimate of the current proton flux and of the accrued and projected proton fluence. When these levels exceed preset thresholds, the computer automatically issues an alert paging members of the operations team, which then convenes to evaluate risk and determine a course of action. Because no single event at current operating altitudes can substantially increase the damage and because intervention costs valuable observing time and re-planning effort, the *Chandra* team only rarely intervenes. On the other hand, if real-time monitoring indicates that radiation levels will trigger autonomous radiation safing (§5.3), there is some economy in observing time and effort to intervene before the EPHIN triggers autonomous action.

5.3. Autonomous safing

As the last line of defense, the EPHIN²³ (§2.3) on-board *Chandra* serves as a radiation monitor. The autonomous-safing strategy is to compare on-board real-time EPHIN data to preset flux thresholds, which trigger autonomous safing against radiation damage. If the flux exceeds any of the thresholds, flight software halts science operations and safes the science instruments. The radiation safing results in the following science-instrument states:

1. ACIS in next-in-line (NIL) position, with video boards powered down.
2. HRC in focus position, with HRC door mostly closed and all high voltage either ramped down or switched off.
3. Objective Transmission Gratings (OTGs) retracted.

Acknowledgements

We thank colleagues at our respective institutions for their contributions. We are especially grateful to Bronek Dichter, Don Brautigam, and Bob Hilmer (AFRL); to Catherine Grant (MIT); to Paul Plucinsky, Eric Martin, Dan Shrophire, Scott Wolk, and Dan Schwartz (CXC); and to Robert Austin (USRA/MSFC). Reinhold Müller-Mellin (EPHIN team, University of Kiel, Germany) contributed greatly to rapid analysis and proper interpretation of the *Chandra* EPHIN data. We also appreciate the generous help of the space-physics and space-environments communities — NOAA Space Environment Center, *ACE* Science Center (Cal Tech), *ACE* Operations Center (GSFC), Johns Hopkins University Applied Physics Laboratory (JHU/APL), Boston University (BU), University of Iowa, Rice University, and others. In particular, we thank the *Geotail* EPIC team (JHU/APL) and the *Polar* CEPPAD team (BU) for providing access to their data sets, and Terry Onsager (NOAA/SEC) for special processing of data at the SEC. Finally, we thank James Ziegler (IBM) for providing the SRIM (Stopping and Range of Ions in Matter) program, including the TRIM (Total Range of Ions in Matter) Monte-Carlo code.

REFERENCES

1. M. C. Weisskopf, H. D. Tananbaum, L. P. Van Speybroeck, and S. L. O'Dell, "Chandra X-Ray Observatory: Overview," in *X-Ray Optics, Instruments, and Missions*, J. Trümper and B. Aschenbach, eds., *Proc. SPIE* **4012**, pp. 2–16, 2000.
2. S. L. O'Dell, M. C. Weisskopf, H. D. Tananbaum, and L. P. Van Speybroeck, "Chandra X-Ray Observatory: Overview," in *X-Ray Optics, Instruments, and Missions IV*, R. B. Hoover and A. B. Walker, eds., *Proc. SPIE* **4138**, 2000, in press.
3. M. C. Weisskopf, S. L. O'Dell, R. F. Elsner, and L. P. Van Speybroeck, "Advanced X-ray Astrophysics Facility (AXAF): An overview," in *X-Ray and Extreme Ultraviolet Optics*, R. B. Hoover and A. B. Walker, eds., *Proc. SPIE* **2515**, pp. 312–329, 1995.
4. M. C. Weisskopf, S. L. O'Dell, and L. P. Van Speybroeck, "Advanced X-ray Astrophysics Facility (AXAF): An overview," in *Multilayer and Grazing Incidence X-Ray/EUV Optics III*, R. B. Hoover and A. B. Walker, eds., *Proc. SPIE* **2805**, pp. 2–7, 1996.
5. S. S. Murray, J. H. Chappell, A. T. Kenter, K. Kobayashi, R. P. Kraft, G. R. Meehan, M. V. Zombeck, G. W. Fraser, J. F. Pearson, J. E. Lees, A. N. Brunton, S. E. Pearce, M. Barbera, A. Collura, and S. Serio, "AXAF High-Resolution Camera (HRC)," in *EUV, X-Ray, and Gamma-Ray Instrumentation for Astronomy VIII*, O. H. Siegmund and M. A. Gummin, eds., *Proc. SPIE* **3114**, pp. 11–25, 1997.
6. S. S. Murray, G. K. Austin, J. H. Chappell, J. J. Gomes, A. T. Kenter, R. P. Kraft, G. R. Meehan, M. V. Zombeck, G. W. Fraser, and S. Serio, "In-flight performance of the Chandra High-Resolution Camera," in *X-Ray Optics, Instruments, and Missions*, J. Trümper and B. Aschenbach, eds., *Proc. SPIE* **4012**, pp. 68–80, 2000.
7. B. E. Burke, J. Gregory, M. W. Bautz, G. Y. Prigozhin, S. E. Kissel, B. B. Kosicki, A. H. Loomis, and D. J. Young, "Soft x-ray CCD imagers for AXAF," *I.E.E.E. Trans. Elec. Devices* **44**, pp. 1633–1642, 1997.
8. M. W. Bautz, M. Pivovarov, F. Baganoff, T. Isobe, S. E. Jones, S. E. Kissel, B. Lamarr, H. L. M. G. Y., P. G. R., Ricker, J. A. Nousek, C. E. Grant, K. Nishikida, F. Scholze, R. Thornagel, and G. Ulm, "X-ray CCD calibration for the AXAF CCD Imaging Spectrometer," in *X-Ray Optics, Instruments, and Missions*, R. B. Hoover and A. B. Walker, eds., *Proc. SPIE* **3444**, pp. 210–224, 1998.
9. D. Heynderickx, B. Quaghebeur, B. Fontaine, A. Glover, W. C. Carey, and E. J. Daly, "New features of ESA's Space Environment Information System (SPENVIS)." ESA Workshop on Space Weather, 1999.
10. G. Y. Prigozhin, S. E. Kissel, M. W. Bautz, C. Grant, B. LaMarr, R. F. Foster, G. R. Ricker, and G. P. Garmire, "Radiation damage in the Chandra x-ray CCDs," in *X-Ray Optics, Instruments, and Missions*, J. Trümper and B. Aschenbach, eds., *Proc. SPIE* **4012**, pp. 720–730, 2000.
11. G. Y. Prigozhin, M. W. Bautz, C. Grant, S. E. Kissel, B. LaMarr, and G. R. Ricker, "Characterization of the radiation damage in the Chandra x-ray CCDs," in *X-Ray and Gamma-Ray Instrumentation for Astronomy XI*, K. A. Flanagan and O. H. W. Siegmund, eds., *Proc. SPIE* **4140**, 2000, these Proceedings.
12. W. C. Blackwell, J. I. Minow, K. Warren, R. M. Suggs, S. L. O'Dell, D. A. Swartz, A. F. Tennant, and S. N. Virani, "Modeling the Chandra space environment," in *X-Ray and Gamma-Ray Instrumentation for Astronomy XI*, K. A. Flanagan and O. H. W. Siegmund, eds., *Proc. SPIE* **4140**, 2000, these Proceedings.
13. J. J. Kolodziejczak, R. F. Elsner, R. A. Austin, and S. L. O'Dell, "Ion transmission to the focal plane of the Chandra X-ray Observatory," in *X-Ray and Gamma-Ray Instrumentation for Astronomy XI*, K. A. Flanagan and O. H. W. Siegmund, eds., *Proc. SPIE* **4140**, 2000, these Proceedings.
14. T. H. Markert, C. R. Canizares, D. Dewey, M. McGuirk, C. S. Pak, and M. L. Schattenburg, "High-energy transmission grating spectrometer for the Advanced X-ray Astrophysics Facility (AXAF)," in *EUV, X-Ray, and Gamma-Ray Instrumentation for Astronomy V*, O. H. Siegmund and J. V. Vallerga, eds., *Proc. SPIE* **2280**, pp. 168–180, 1994.
15. D. Dewey, K. A. Flanagan, H. L. Marshall, C. Baluta, C. R. Canizares, D. S. Davis, J. E. Davis, T. T. Fang, D. P. Huenemoerder, J. H. Kastner, N. S. Schulz, M. W. Wise, J. J. Drake, J. Z. Juda, M. Juda, A. C. Brinkman, C. J. T. Gunsing, J. S. Kaastra, G. Hartner, and P. Predehl, "Towards the calibration of the HETGS effective area," in *Grazing Incidence and Multilayer X-Ray Optical Systems*, R. B. Hoover and A. B. Walker, eds., *Proc. SPIE* **3113**, pp. 144–159, 1997.
16. R. F. Elsner, J. J. Kolodziejczak, S. L. O'Dell, D. A. Swartz, A. F. Tennant, and M. C. Weisskopf, "Measurements with the Chandra X-Ray Observatory's flight contamination monitor," in *X-Ray Optics, Instruments, and Missions*, J. Trümper and B. Aschenbach, eds., *Proc. SPIE* **4012**, pp. 612–618, 2000.

17. R. F. Elsner, J. J. Kolodziejczak, S. L. O'Dell, D. A. Swartz, A. F. Tennant, and M. C. Weisskopf, "Measurements with the Chandra X-Ray Observatory's flight contamination monitor," in *X-Ray Optics, Instruments, and Missions IV*, R. B. Hoover and A. B. Walker, eds., *Proc. SPIE* **4138**, 2000, in press.
18. R. F. Elsner, M. K. Joy, S. L. O'Dell, B. D. Ramsey, and M. C. Weisskopf, "Ground-to-orbit transfer of the AXAF-I flux scale: In-situ contamination monitoring of x-ray telescopes," in *Multilayer and grazing incidence X-ray/EUV optics for astronomy and projection lithography*, R. B. Hoover and A. B. Walker, eds., *Proc. SPIE* **2279**, pp. 332–342, 1994.
19. R. F. Elsner, S. L. O'Dell, B. D. Ramsey, A. F. Tennant, M. C. Weisskopf, J. J. Kolodziejczak, D. A. Swartz, D. E. Engelhaupt, G. P. Garmire, J. A. Nousek, M. W. Bautz, T. J. Gaetz, and P. Zhao, "Calibration results for the AXAF flight contamination monitor," in *X-Ray Optics, Instruments, and Missions*, R. B. Hoover and A. B. Walker, eds., *Proc. SPIE* **3444**, pp. 177–188, 1998.
20. K. Gendreau, M. Bautz, and G. Ricker, "Proton damage in x-ray CCDs for space applications: Ground evaluation techniques and effects on flight performance," *Nuclear Instruments and Methods in Physics Research, A* **335**, pp. 318–327, 1993.
21. A. Holland, "The effect of bulk traps in proton irradiated EEV CCDs," *Nuclear Instruments and Methods in Physics Research, A* **326**, pp. 335–343, 1993.
22. T. Hardy, R. Murowinsky, and M. Deen, "Charge transfer efficiency on proton damaged CCDs," *IEEE Transactions on Nuclear Science* **40**, pp. 154–163, 1998.
23. R. Müller-Mellin, H. Kunow, V. Fleissner, E. Pehlke, E. Rode, N. Roschmann, C. Scharmberg, H. Sierks, P. Ruzsnyak, I. E. S. McKenna-Lawlor, J. Sequeiros, D. Meziat, S. Sanchez, J. Medina, L. der Peral, M. Witte, R. Marsden, and J. Henrion, "COSTEP — comprehensive suprathermal and energetic particle analyzer," *Solar Physics* **162**, pp. 483–504, 1995.
24. M. S. Gussenhoven, E. G. Mullen, M. D. Violet, C. Hein, J. Bass, and D. Madden, "CRRES high-energy proton flux maps," *IEEE Trans. Nuclear Science* **40**, pp. 1450–1457, 1993.
25. N. Virani, R. Müller-Mellin, P. P. Plucinsky, and Y. M. Butt, "Chandra X-ray Observatory's radiation environment and the AP-8/AE-8 model," in *X-Ray Optics, Instruments, and Missions*, J. Trümper and B. Aschenbach, eds., *Proc. SPIE* **4012**, pp. 669–680, 2000.
26. D. J. Williams, R. W. McEntire, C. Schlemm II, A. T. Y. Lui, G. Gloeckler, S. P. Christon, and F. Gliem, "Geotail Energetic Particles and Ion Composition instrument," *J. Geomag. Geoelect.* **46**, pp. 39–57, 1994.
27. A. Nishida, K. Uesugi, I. Nakatani, T. Mukai, D. H. Fairfield, and M. H. Acuna, "Geotail mission to explore earth's magnetotail," *Eos* **73**, pp. 425–427, 1992.
28. A. Nishida, "The Geotail mission," *Geophysical Research Letters* **21**, pp. 2871–2873, 1994.
29. R. D. Zwickl, K. A. Doggett, S. Sahm, W. P. Barrett, R. N. Grubb, T. R. Detman, V. J. Raben, C. W. Smith, P. Riley, R. E. Gold, R. A. Mewaldt, and S. Maruyama, "The NOAA Real-Time Solar-Wind (RTSW) system using ACE data," *Space Science Reviews* **86**, pp. 633–648, 1998.
30. E. C. Stone, A. M. Frandsen, R. A. Mewaldt, E. R. Christian, D. Margolies, J. F. Ormes, and F. Snow, "The Advanced Composition Explorer," *Space Science Reviews* **86**, pp. 1–22, 1998.
31. R. E. Gold, S. M. Krimigis, S. E. Hawkins III, D. K. Haggerty, D. A. Lohr, E. Fiore, T. P. Armstrong, G. Holland, and L. J. Lanzerotti, "Electron, Proton and Alpha Monitor on the Advanced Composition Explorer spacecraft," *Space Science Reviews* **86**, pp. 541–562, 1998.
32. D. J. McComas, S. J. Bame, P. Barker, W. C. Feldman, J. L. Phillips, P. Riley, and J. W. Griffee, "Solar Wind Electron Proton Alpha Monitor (SWEPAM) for the Advanced Composition Explorer," *Space Science Reviews* **86**, pp. 563–612, 1998.
33. C. W. Smith, J. L. Heureux, N. F. Ness, M. H. Acuña, L. F. Burlaga, and J. Scheifele, "The ACE magnetic fields experiment," *Space Science Reviews* **86**, pp. 613–632, 1998.
34. K. A. Costello, "Moving the Rice MSFM into real-time forecast mode using solar-wind driven forecast models." Ph. D. dissertation, Rice University, June 1997.
35. E. C. Stone, C. M. S. Cohen, W. R. Cook, A. C. Cummings, B. Gauld, B. Kecman, R. A. Leske, R. A. Mewaldt, M. R. Thayer, B. L. Dougherty, R. I. Grumm, B. D. Milliken, R. G. Radocinski, M. E. Wiedenbeck, E. R. Christian, S. Shuman, and T. T. von Rosenvinge, "The Solar Isotope Spectrometer for the Advanced Composition Explorer," *Space Science Reviews* **86**, pp. 357–408, 1998.
36. J. Ziegler, J. Beirsack, and U. Littmark, *The Stopping Power of Ions in Solids*, Pergamon Press, New York, New York, 1996.